Mitophagy Eliminates the Accumulation of SARM1 on the Mitochondria, Alleviating Axon Degeneration in Acrylamide Neuropathy

Shuai Wang
Shandong University Cheeloo College of Medicine https://orcid.org/0000-0003-3533-8565
Hui Yong
Shandong University Cheeloo College of Medicine
Cuiqin Zhang
Shandong University Cheeloo College of Medicine
Kang Kang
Shandong University Cheeloo College of Medicine
Mingxue Song
Shandong University Cheeloo College of Medicine
Yiyu Yang
Shandong University Cheeloo College of Medicine
Zhengcheng Huang
Shandong University Cheeloo College of Medicine
Shu'e Wang
Shandong University Cheeloo College of Medicine
Haotong Ge
Shandong University Cheeloo College of Medicine
Xiulan Zhao
Shandong University Cheeloo College of Medicine
Fuyong Song (fysong3707@sdu.edu.cn)
Shandong University Cheeloo College of Medicine https://orcid.org/0000-0003-2662-8210

Research article

Keywords: Acrylamide, Mitophagy, Mitochondrial dynamics, Mitochondrial quality control, Peripheral neuropathy, PINK1, Rapamycin, SARM1, Wallerian degeneration,

Posted Date: December 13th, 2021

DOI: https://doi.org/10.21203/rs.3.rs-1113241/v1

Abstract

Background: Sterile-α and toll/interleukin 1 receptor motif containing protein 1 (SARM1) is the central executioner of axon degeneration. Although it has been confirmed to have a mitochondrial targeting sequence and can bind to and stabilize PINK1 on depolarized mitochondria, the biological significance for mitochondrial localization of SARM1 is still unclear. Chronic acrylamide (ACR) intoxication can cause typical pathology of axonal injury, owning the potential to explore the interaction between mitochondria and SARM1 during the latent period of axon destruction.

Methods: The expression and the mitochondria distribution of SARM1 were evaluated in *in vivo* and *in vitro* ACR neuropathy models. Transmission electron microscopy, immunoblotting, and immunofluorescence were performed to evaluate mitochondrial dynamics and PINK1-dependent mitophagy. LC3 turnover experiment and live cell imaging were conducted to further assess the state of mitophagy flux. In order to verify the effect of mitophagy in SARM1-mediated axon degeneration, low-dose and low-frequency rapamycin was administered in ACR-exposed rats to increase basal autophagy.

Results: In a time- and dose-dependent manner, ACR induced peripheral nerve injury in rats and truncated axons of differentiated N2a cell. Moreover, the severity of this axon damage was consistent with the up-regulation of SARM1. SARM1 prominently accumulated on mitochondria, and at the same time mitophagy was activated. Importantly, rapamycin (RAPA) administration eliminated mitochondrial accumulated SARM1 and alleviated SARM1 dependent axonal degeneration.

Conclusions: Complementing to the coordinated activity of NMNAT2 and SARM1, mitochondrial localization of SARM1 may be part of the self-limiting molecular mechanisms of Wallerian axon destruction. In the early latent period of axon damage, the mitochondrial localization of SARM1 will help it to be isolated by the mitochondrial network and to be degraded through PINK1-dependent mitophagy to maintain local axon homeostasis. When the mitochondrial quality control mechanisms are broken down, SARM1 will cause irreversible damage for axon degeneration. Moderate autophagy activation can be invoked as potential strategies to alleviate axon degeneration in ACR neuropathy and even other axon degeneration diseases.

Background

Axon degeneration is a common hallmark of neuropathies, traumatic injury, and multiple neurodegenerative disorders. The molecular mechanism of axon degeneration has been primarily elucidated through the study of Wallerian axon destruction pathway. Wallerian degeneration, first described by the British neurophysiologist Augustus Waller in 1849 (1), refers to rapid axonal fragmentation after a long period of relative latency due to a genetically encoded self-destruction program that is activated distal to the point of the axon cut site (2–4). This is the most extreme and typical manifestation of axon degeneration. Over the past decades, great progress has been made in the understanding of this active process. The coordinated activity of both the pro-survival factors and the

pro-degeneration factors, exemplified by nicotinamide mononucleotide adenyltransferase 2 (NMNAT2) and sterile-α and toll/interleukin 1 receptor motif containing protein 1 (SARM1), limits degeneration signaling in an “off” state in healthy axons. After axotomy, NMNAT2 is rapidly consumed in the axon segment distal to the injury site due to the interruption of axon transport and the degradation (5, 6), resulting in the hindrance of nicotinamide adenine dinucleotide (NAD+) synthesis. The disruption of NAD+ synthesis will increase the amount of nicotinamide mononucleotide (NMN), the precursor of NAD+, in the axon. The raised ratio of NMN and NAD+ (7) activates SARM1, which further consumes NAD+ to switch into the irreversible stage accompanied by adenosine triphosphate (ATP) depletion, neurofilament hydrolysis, and axon fragmentation (8).

SARM1 is the defining molecule of axon destruction. Activation of SARM1 triggers metabolic catastrophe and axon destruction, whereas genetic deletion protects axons from various injury (9). As the central executioner of axon degeneration, SARM1 is evolutionarily highly conserved, having homologues in mouse, Drosophila, zebrafish, Caenorhabditis elegans, amphioxus, and horseshoe crab (10–13). These homologues share a common domain architecture constituted of autoinhibitory N-terminal armadillo motifs (ARM), tandem sterile α motif (SAM) domains that mediate constitutive homomultimerization, and a C-terminal toll/interleukin 1 receptor (TIR) domain. The N-terminal SAM-TIR domain has NAD+ cleaving activity, and the activation induces axonal NAD+ depletion that is followed by ATP loss. So far, although we have a preliminary understanding of these domains, the function of SARM1 and its regulatory mechanisms still needs to be further studied. It is currently believed that elucidating the exact subcellular localization of SARM1 will offer insights into its functional role. Even though it remains to be defined, mitochondrial localization has been proposed. The N-terminal 27 amino acids of SARM1 are hydrophobic polybasic and have the capacity to fold into an α-helix that is required for association with the mitochondrial outer membrane. It serves as a mitochondria-targeting sequence, associating SARM1 to the mitochondria (14).

SARM1 and mitochondria are intimately connected. In addition to structural biological evidence that SARM1 has a mitochondrial import sequence, the two also have a metabolic connection. ATP produced in mitochondria provides energy for NAD+ synthesis (15), and NAD+ plays an important role in both oxidative phosphorylation and glycolysis (16, 17). NAD+ metabolic disorder is a necessary and sufficient condition for the activation of SARM1. The activated SARM1 with the NAD+ cleavage site exposed, consumes NAD+, accelerates energy exhaustion and initiates axon fragmentation. Indeed, ATP depletion is a defining indicator of the transition from the latent period to the irreversible period of Wallerian degeneration (8, 9). However, previous studies have shown that Wallerian degeneration is only modestly influenced by mitochondria (18). The biological significance of SARM1 mitochondrial localization has yet to be further explored.

To identify conditions that would benefit from blocking SARM1 dependent Wallerian axon destruction pathway, peripheral neuropathies are re-examined. Here, we want to explore whether the SARM1 dependent axon degeneration mechanism is involved in peripheral nerve damage in ACR poisoning? Further, if SARM1 is activated in this progress, are there any potential regulatory mechanisms?

As the vinyl monomer for the production of polyacrylamide, ACR is widely utilized in a variety of industrial settings and laboratories (19). In addition to occupational exposure, ACR in food, drinking water, coffee, and cigarette smoke has a potential hazard to the general population (20–23). In June 2002, a risk assessment of ACR in food was conducted in the joint Food and Agriculture Organization of the United Nations (FAO) and the World Health Organization (WHO) consultation. In reports of the Joint FAO/WHO Expert Committee on Food Additives (JECFA), the potential adverse neurological effects were noted among individuals with high dietary exposure to ACR. Chronic ACR intoxication induces peripheral neuropathy in people (24–27) and animals (28, 29), which are characterized by progressive axon degeneration of the distal ends of the longest and the largest nerve fibres. As exposure continues, progressive retrograde destruction of these distal axon regions ensues with preservation of more proximal segments resulting symptoms, that is, ataxia, skeletal muscle weakness and numbness of the hands and feet. The specific spatiotemporal pattern of axon damage is similar to the profile of Wallerian degeneration after axotomy (30–34) and is named as Wallerian-like degeneration. Studying the changes of SARM1 in such a slowly progressing and moderate axon destruction process will contribute to enhancing the understanding of Wallerian degeneration and explore its potential regulatory mechanism.

Methods

Animals and treatments

Adult male Wistar rats (160-180g, SPF) were supplied by Jinan Pengyue Laboratory Animal Breeding Co., Ltd., Jinan, China. All animals were kept in a barrier system. Food and drinking water were available. The animal room was maintained at approximately 22 ℃ and 50% humidity with a 12 h light/dark cycle. After seven days of acclimatization, rats were randomly divided into groups for experiments. With references to ACR intoxication regimens (35), the *in vivo* ACR neuropathy model set up four groups of control, low, medium, and high doses, 0, 10, 20 and 40 mg/kg b.w. i.p. every other day, respectively. RAPA intervention experiment had the same ACR dose of the high dose group. The dose of RAPA was 1 mg/kg b.w. i.p. once per week. ACR was dissolved in saline. And the control group was treated with saline. RAPA was dissolved in DMSO, sequentially added with PEG300 and Tween-80 to help dissolve, and diluted with physiological saline (volume ratio: DMSO 2.5%, PEG300 10%, Tween-80 1.25%, saline 86.25%) to get a clear liquid.

Neurobehavioral and neurophysiological tests

Rotarod latency test

ZS-ROM rotarod fatigue equipment (Beijing Zhongshidichuang Technology and Development Co., Ltd., Beijing, China) was utilized. All rats received training before intoxication, that was, staying on the equipment for 60 s at a velocity of 8 rpm. During the formal test, the original velocity was set at 0 rpm and accelerated smoothly to 40 rpm within 200 s. The time that animals stayed on the rod was recorded as its latency to fall (36, 37).

Landing foot splay measuring

Landing foot splay was the distance between the inner surfaces of the fourth digits of each foot after the animals were dropped from a 30 cm height (38).

Gait score evaluation

Rats were positioned in an open field and were observed for 3 min. Following the observation, a gait score was assigned from 1 to 4 where 1 = a normal, unaffected gait; 2 = a slightly abnormal gait (tiptoe walking, hindlimb adduction); 3 = moderately abnormal gait (obvious movement abnormalities characterized by dropped hocks and tail dragging); 4 = severely abnormal gait (dragging hindlimbs and complete absence of rearing) (39, 40).

Motor nerve conduction velocity measurement

The motor nerve conduction velocity of the rat tail was measured with a BL-420E biological function experimental system (Chengdu Taimeng Technology Co., Ltd., Chengdu, China). The electrodes used in our experiments were stainless steel needles, 0.34 mm in diameter and about 15 mm long. The rat was fixed in the supine position and its tail was exposed to a pair of stimulating electrodes, which were connected to the two pairs of sensor electrodes, and an earth electrode. A single electric stimulus of 5 V was applied through the stimulating electrodes and two action potential oscillogram curves were recorded. The time between the two peak points and the distance between the two negative sense electrodes was recorded to calculate the motor nerve conduction velocity (41).

Cell culture and treatments

Mouse Neuro2a (N2a) neuroblastoma cells, purchased from American type culture collection (ATCC, USA), were cultured in high-glucose Dulbecco's Modified Eagle's medium (DMEM) supplemented with 10% (v/v) fetal bovine serum (FBS), 1% penicillin-streptomycin, 1% MEM Non-Essential Amino Acids (NEAA) and 1% sodium pyruvate at 37°C in a 5% CO2 incubator. For differentiation, cells were induced in DMEM medium supplemented with 2% (v/v) FBS and 10 μM retinoic acid for 48 h. Then, differentiated cells were treated with ACR.

Cytotoxicity test and cellular morphology

Cytotoxicity test was conducted by Cell Counting Kit-8 (CCK8) (Tecan Infinite® M200 Pro). Axons of ACR treated N2a cells were observed by microscope (Nikon ECLIPSE Ti). In each group, we observed 10 fields and recorded the length of six axons by TCapture at least for each field. The images shown in the article have been faded and contrast enhanced to increase the accuracy of the measurement. Adjustments were applied to the entire image. Based on the results of the cytotoxicity test and cellular morphology, differentiated N2a cells began to show damage after being treated with 0.5 mM ACR for 24 h, and had obvious axon degeneration after being treated with 2.0 mM ACR for 24 h.

LC3 turnover experiment

Cells were seeded in six-well plates, adhered, differentiated, and pre-treated with 10 μg/mL Pepstatin A and E64d for 1 h before treatment with ACR (42, 43).

Pathological examination

Histopathological examination

Rats were anesthetized with a 1:1 mixture of 5% chloral hydrate and 12.5% urethane. After infusion of saline and 4% paraformaldehyde solution, the tissues were quickly dissected and separated. Spinal lumbosacral enlargements (L2-S3) were fixed in 4% paraformaldehyde for 48 h, dehydrated in alcohol, and then embedded in paraffin. Every 20th cross section (5 μm) was processed by haematoxylin and eosin (H&E) and Nissl staining (0.5% Thionine solution), scanned as digital slices through Olympus VS120, and analyzed blindly. Cells with a distinct nucleus and a diameter of at least 25 μm located in the anterior horn ventral to the line tangential to the ventral tip of the central canal were considered to be α motor neurons. Those α motor neurons with abnormal morphological changes, such as hyperchromatic cytoplasm, were counted.

Immunofluorescence staining

N2a cells were seeded on sterile cover glasses placed in the 24-well plates. After desired treatment, N2a cells adherent on glasses were washed with phosphate buffered solution (PBS) twice. Then, cells were fixed in 4% paraformaldehyde solution for 10 min, quenched by 50 mM NH_4Cl/PBS for 10 min, permeabilized by 50 μg/ml Digitonin/PBS for 5 min, and blocked by 1% Gelatin/PBS for 30 min at 4°C. Between each step, the glasses were washed by PBS. Then, cells were stained with antibodies dilutions (1:200) at 4°C overnight. After washing with PBS, cells were incubated with goat secondary antibody dilutions (1:1000) at room temperature for 1 h. Finally, cells were observed by a Nikon fluorescence microscope. Paraffin tissue sections were dewaxed, hot fixed, and stained as mentioned above. Fiji Image-J was utilized to perform co-localization analysis of fluorescence images, including the Pearson's R value calculation of the entire image and gray intensity analysis of the region of interest.

Transmission electron microscopy ultrastructure analysis

After perfusion, spinal cord (L2-S3) and sciatic nerve (sciatic notch-popliteal fossa) were separated, trimmed to the appropriate size in 2.5% glutaraldehyde droplets, and fixed. Following ultramicrotomy, the sections were transferred on to a nickel grid and stained with osmium tetroxide, uranyl acetate and lead citrate. The samples were subsequently observed using a JEM1010 transmission electron microscope (Jeol).

Live cell imaging of N2a cells

Mito Tracker Green FM staining was applied to visualize mitochondria, and Lyso Tracker Red DND-99 to mark lysosomes and other acidic organelles. Hoechst 33342 was used to stain nuclei. Following the user guide, Mito Tracker Green FM and Lyso Tracker Red DND-99 were dissolved in high-quality, anhydrous DMSO to prepare a 1 mM stock solution and were stored at −40°C. The Stock solutions of Mito Tracker

Green FM and Lyso Tracker Red DND-99 were diluted with DMED to a final concentration of 100 nM and 50 nM, respectively. N2a cells treated with 2 mM ACR for 24 h or not were incubated with this working solution for 30 min, and then imaged by a fluorescence microscope.

Western blotting

Mitochondrial fractionation

Mitochondria were isolated using a Mitochondria Isolation Kit by sequential centrifugation. Briefly, samples were homogenized and were lysed by Mitochondria Isolation Solution supplemented with protease inhibitor cocktail and phosphatase inhibitor cocktail. Lysates were centrifuged at 1,000 g for 5 min to remove the plasma membrane fraction, and subsequently, the supernatants were centrifuged at 3,500 g for 10 min to get purified mitochondria. Isolated mitochondrial pellets were lysed and subject to immunoblot analysis. Given the low yield of mitochondrial fraction and consistency changes of Wallerian degeneration related molecular in the spinal cord and sciatic nerve, we did not extract the mitochondrial components of the sciatic nerve homogenate.

Samples preparation, electrophoresis, and immunoblotting

The sciatic nerve was ground into powder in liquid nitrogen and the immunoblotting sample was prepared according to the subsequent steps. The spinal cord was homogenized directly in ice-cold RIPA buffer supplemented with protease inhibitor cocktail and phosphatase inhibitor cocktail. Then, homogenates were centrifuged at 12,000 g for 10 min. Supernatants were used for immunoblotting analysis. After protein concentration was determined by BCA™ Protein assay Kit, the sample was mixed with 4x loading buffer, and then heated at 100°C for 5 min.

To assess relative changes in protein content, corresponding protein samples were subjected to sodium dodecyl sulfonate-polyacrylamide gel electrophoresis. Following electrophoresis, proteins were transferred electrophoretically to polyvinylidene fluoride membranes. Then the membranes were blocked with 3% fat-free milk for 45 min and incubated with primary antibody (**Additional file 1. Reagent**) diluted in 0.1% BSA for 8 h. Following primary antibody, membranes were washed in a mixture of Tween 20 and tris-buffered saline and incubated with horseradish peroxidase-conjugated secondary antibody at room temperature for 1 h. After being washed again, the membranes were incubated by using the SuperSignal West Pico Chemiluminescent Substrate reagents for 2 min and then exposed to Tanon-5200 Multi Chemiluminescence Imaging System (Tanon Science & Technology, Shanghai, China). The full-blot images can be found in the additional file (**Additional file 2. Original blots**). Digitized data were quantified as integrated optical density using Fiji Image-J (44). Each protein was repeated at least three times. VDAC and β-actin (voltage-dependent anion-selective channel) were detected as loading control for total proteins and mitochondrial proteins respectively.

Statistical analysis

The performers were blinded to the experimental design in data collection and analysis. Data are presented as means ± standard error of the mean (SEM) after analysis using SPSS 18.0 software. Two-way Repeated Measures ANOVA was used for neurobehavioral data. Unpaired t test, one-way ANOVA and two-way ANOVA followed by Bonferroni's post-hoc test, were performed in the right situation (**Additional file 3. Statistical analyses**). The differences were considered significant at $p<0.05$.

Results

SARM1 dependent Wallerian degeneration is involved in ACR neuropathy

A rat ACR neuropathy model was established after four weeks of exposure to ACR (0, 10, 20 and 40 mg/kg b.w. i.p. every other day, Fig. S1A). The symptoms of peripheral nerve injury were evaluated by neurobehavioral performances (Fig. 1A). After three weeks of intoxication, rats in the high-dose group had produced a triad of neurological deficits with decreased rotarod staying time, increased landing foot splay distances, and increased gait score. Consistent with neurobehavioral indicators, Axon destruction was seen in rats subjected to ACR for four weeks (Fig. 1B-E). Compared with the age-matched control group, the sciatic nerve axons in rats exposed to ACR for four weeks were lost. The retained axons were swollen with an increased diameter and myelin sheaths were loose (Fig. 1B, 1C). Furthermore, the motor nerve conduction velocity slowed down in a dose-dependent manner (Fig. 1D). The α motor neurons in the lateral anterior horn of the spinal cord, innervating transarticular extrafusicular muscle fibres through axons in the sciatic nerve, also showed obvious morphological changes. And the number of abnormal neurons with morphological changes, such as hyperchromatic cytoplasm, increased in a dose-dependent manner (Fig. 1B, 1E, Fig. S1B). Interestingly, these abnormal α motor neurons did not over-express RIPK1 and be negative for TUNEL staining (Fig. S1C, S1D), indicating that they did not die even though they were under stress. Survival neurons with damaged axons revealed the early morphological feature for ACR neuropathy, the axon degeneration. Moreover, Wallerian degeneration-related molecules were detected by Western blotting. The constant up-regulation of SARM1 in the spinal cord and sciatic nerve (Fig. 1F, 1G) suggested that the SARM1 dependent Wallerian axon destruction pathway was activated in ACR-induced axon degeneration.

In order to directly observe the axon degeneration caused by ACR, we then measured the axon length of N2a cells processed by ACR for different concentrations and different time (Fig. S1E, S1F). The axons were observed shortened, accompanied by swelling, blebbing and fragmentation (Fig. 1H, 1I). The expression of SARM1 was also up-regulated similarly to that *in vivo*, and it was dose- and time-dependent (Fig. 1J).

Taken together, both the spatiotemporal pattern of axon degeneration and the SARM1 dependent neuropathy indicated that ACR intoxication triggered the activation of Wallerian degeneration machinery.

The up-regulated SARM1 accumulates on mitochondria

Immunofluorescence was then conducted to determine the intracellular localization of SARM1. As demonstrated in Fig. 2A, SARM1 aggregated into puncta along the nerve fibres, and even translocated in the soma of α motor neurons from rats exposed to ACR for four weeks. Combined with the research on the subcellular localization of SARM1, we speculated that these plaque-like and punctate structures may be linked to the mitochondrial localization of SARM1. Then, we quantified mitochondrial SARM1 by isolating the mitochondrial fraction. In the low-dose group, SARM1 in the mitochondria fraction changed significantly, despite that the cytoplasmic level was unchanged (Fig. 2B). Compared with the changes in the cytoplasm, the more obvious alteration was observed in the mitochondria fraction of the higher dose groups further confirming the accumulation of SARM1 on mitochondria (Fig. 2B). The immunofluorescence co-localization analysis of SARM1 and Parkin further proved the above conclusion (Fig. 2C). In the low-dose group, the co-localization of SARM1 and Parkin dramatically increased along axons. With increasing exposure doses, the degree of co-localization in axons increased. And evident co-localization was found in α motor neuron cell bodies for the high-dose group. Finally, *in vitro* experiments also verified the mitochondrial aggregation of SARM1 (Fig. 2D). The immunofluorescence of SARM1 presented as dots in ACR treated N2a cells. The co-localization degree of SARM1 with mitochondrial molecules, e.g. Parkin and DRP1, also markedly increased, indicating that SARM1 got enriched on mitochondria (Fig. S2A, S2B). Next, our research focused on the role of mitochondria in ACR-induced Wallerian-like degeneration.

Mitochondrial dynamics are disturbed and mitophagy is activated

Transmission electron microscopy analysis demonstrated that there were a large number of organelles in the swollen axons from rats exposed to ACR for four weeks, including fragmented mitochondria and some autophagy-related structures (Fig. 3A). The morphological changes of mitochondria in the spinal cord and sciatic nerve were similar. The mitochondria in ACR treated groups were spherical and elliptical with severely disorganized and swollen cristae, while the mitochondria in the control formed short tubules with a clear sheet-like structure of mitochondrial cristae. Analysis of those images showed that ACR caused an increase in the mitochondrial number, but the length of mitochondria was shortened. The frequency distribution of mitochondrial length for ACR-treated rats was concentrated in a shorter area (Fig. 3B). Western blotting results were in agreement with the morphological findings, disclosing the fragmentation trend of the mitochondrial network. The protein levels of DRP1 and p-DRP1 (Ser616), which promote mitochondrial fission, were raised significantly in the mitochondrial fraction. By contrast, the proteins involved in mitochondrial fusion, e.g. Mfn2 and OPA1, were markedly reduced (Fig. 3C). Furthermore, western blotting also illustrated that PINK1, Parkin, OPTN, NDP52, LC3-□, LC3-□/□ and P62 increased dramatically in ACR-intoxicated rats (Fig. 3D, 3E). The immunofluorescence results were in accord with this (Fig. 3F, Fig. S3).

Similarly, *in vitro* experiments also supported that ACR up-regulated mitophagy-related proteins (Figure 4A). To ascertain the alteration of autophagic flux, we performed an LC3 turnover experiment in N2a cells

(Fig. 4B). Pre-treatment with lysosome inhibitor Pepstatin A and E-64d further elevated the levels of LC3-Ⅱ, LC3-Ⅱ/Ⅰ, and P62 confirming that ACR induced autophagy with the autophagic flux increased on-rate. In addition, the overlap of mitochondrial marker and intracellular acidic organelle marker greatly increased in ACR treated N2a cells through live cell imaging of Mito Tracker Green FM and Lyso Tracker Red DND-99 (Fig. 4C). Moreover, the co-localization of PINK1 and Tom20 (Fig. 4D), LC3 and Tim23 (Fig. 4E) increased in ACR treated cells. These results fully indicated that ACR activated mitophagy.

Rapamycin intervention clears mitochondria accumulated SARM1 and partly alleviates ACR neuropathy

Mitophagy selectively degrades defective mitochondria to maintain the mitochondrial network in a fine state. To verify the negative feedback inhibition of mitophagy on mitochondrial aggregated SARM1, we conducted a RAPA intervention experiment (Fig. S5A). Rats in the intervention group were addressed in low-dose, low-frequency RAPA to improve basal autophagy and to limit possible adverse effects. Compared with the ACR-intoxication group, abnormal neurobehavioral performances in the RAPA intervention group were delayed, and the severity was lower (Fig. 5A). Furthermore, pathological injuries of axons and α motor neurons were improved (Fig. 5B-D), indicating that ACR-induced Wallerian-like degeneration was significantly alleviated following RAPA intervention. Nerve conduction velocity was also obviously improved (Fig. 5E). The aggregation of SARM1 on the mitochondria was considerably decreased (Fig. 5F), and mitochondrial dynamics- and mitophagy-related proteins returned to nearly normal levels (Fig. 5F, Fig. S5B). More importantly, the shape, number, length, and length distribution of mitochondria in the RAPA intervention group recovered with the elimination of mitochondrial SARM1 (Fig. 5G, 5H, Fig. S5C). The results suggested that autophagy activator RAPA partially rescued the phenotype of ACR neuropathy.

Discussion

Neurotoxicity is the quintessential effect of ACR, and Wallerian-like degeneration is typical pathological change of chronic ACR intoxication. In this study, we analyzed ACR-induced axon degeneration *in vivo* and *in vitro*, confirming that the SARM1-dependent Wallerian axon destruction pathway was associated with peripheral nerve damage in ACR poisoning. These results not only confirmed the neuropathology of ACR intoxication, but also lead to the development of promising therapeutic strategies.

Furthermore, we found that ACR induced obvious accumulation of SARM1 on mitochondria. Mitochondrial quality control mechanisms, e.g. mitochondrial dynamics and the PINK1-dependent mitophagy pathway, changed. Finally, pharmacological activation of autophagy by RAPA effectively removed SARM1 which accumulated on the mitochondria and partly alleviated axon degeneration. These findings indicated that mitophagy limits Wallerian degeneration through the clearance of the pro-degenerative factor SARM1 in ACR peripheral neuropathy.

The mitochondrial localization of SARM1 may involve in mitochondrial neurites distribution, anoxic degeneration (45) and neuronal survival regulations (46–48). But other studies prove that deletion of the mitochondrial localization sequence does not alter its ability to promote axon destruction (49). We consider that these inconsistent results may be ascribed to differences in the type of injury, the dose, and the course of the disease. The Wallerian degeneration models of axotomy (18) or chemotherapy-induced peripheral neuropathy, e.g. vincristine, bortezomib and paclitaxel (50, 51), induce rapid axon degeneration with a relatively short latent period, making it difficult to observe the interaction between mitochondrial quality control and SARM1 in the early incubation stage. The results in this study preliminarily confirmed that ACR could induce the SARM1 dependent axon degeneration. Moreover, the level of NMNAT2 did not decrease (Fig. 1F, G) as in the active degeneration stage. The relevant multi-omics data suggest that the NAD+ level in the ACR-intoxication model is still maintained at a relatively high level (Fold Change of the Control = 0.79, p = 0.005, FDR = 1.61%) (52), instead of depleted by increased SARM1. Although it is not ruled out that some axons have entered the active degeneration stage and lost, these above indicate that there are axons still in the early latent stage of axon destruction in rats subjected to ACR for four weeks. This provides the possibility to fully explore the potential biological significance of SARM1 mitochondrial localization. Combined with our results, mitochondrial localization of SARM1 is likely to be related to its clearance through the mitophagy pathway, which may explain these seemingly contradictory observations.

Mitochondria are dynamic organelles. They are actively recruited to specific cellular locations, fuse and divide continually which serves to intermix the lipids and contents of a population of mitochondria, and have dynamic structures under fine quality control conditions (53–56). At present, increasing evidence support that macroautophagy/autophagy is involved in the process of axon degeneration (57–61). And mitophagy, a specific type of autophagy that selectively degrades defective mitochondria, has received extra attention in energy maintenance for damaged axons. PINK1 dependent pathway is one of the best-studied mitophagy mechanisms (62–65). PINK1 is a serine/threonine kinase with an N-terminal mitochondrial targeting sequence. Selective accumulation of PINK1 on the dysfunctional mitochondria can recruit Parkin, OPTN, NDP52 etc., and these binding partners, in turn, induce the degradation of the damaged mitochondria. Previous studies have found that SARM1 in the mitochondrial outer membrane contributes to the stabilization of PINK1 and induces mitophagy (66). Therefore, mitochondrial localization of SARM1 will help to sequester the cytoplasm SARM1 through the mitochondrial dynamic process, and to the final degradation by mitophagy in ACR peripheral neuropathy. This is also consistent with the related results of RAPA intervention.

Conclusions

Taken together, the study here finds that the up-regulated SARM1 induced by ACR intoxication accumulates on mitochondria with the N-terminal mitochondrial targeting sequence, which stabilizes PINK1 and triggers the mitophagy degradation machinery. Mitophagy clearance of SARM1 is complementary to the coordinated activity of NMNAT2 and SARM1. Enhancements of mitophagy with pharmacological methods will promote the clearance of SARM1 and prevent it from breaking down NAD+

metabolism, mitochondrial quality control, and other homeostasis mechanisms. Our research preliminarily demonstrated the potential role of mitophagy in ACR-induced toxic peripheral neuropathy. Further elucidating the mechanistic link between mitophagy and SARM1-dependent axon degeneration will help to develop new strategies for the prevention and treatment of a variety of axon destruction diseases.

Abbreviations

ACR	acrylamide;
ARM	armadillo motifs;
ATP	adenosine triphosphate;
NAD+	nicotinamide adenine dinucleotide;
NMN	nicotinamide mononucleotide;
NMNAT2	nicotinamide mononucleotide adenyltransferase 2;
RAPA	Rapamycin;
SAM	sterile α motif;
SARM	sterile-α and toll/interleukin 1 receptor motif containing protein 1;
TIR	TIR: toll/interleukin 1 receptor;

Declarations

Ethics approval and consent to participate

Animals were treated according to the NIH Guide for Care and Use of Laboratory Animals and followed the principles in the "Use of Animals in Toxicology". All protocols were approved by the Institutional Animal Care and Use Committee of Shandong University.

Consent for publication

Not applicable.

Availability of data and materials

The datasets used and/or analysed during the current study are available from the corresponding author on reasonable request.

Competing interests

The authors declare that they have no competing interests.

Funding

This work was supported by the National Natural Science Foundation of China (No. 82173552; No. 81673209).

Authors' contributions

S Wang, a major contributor in writing the manuscript, performed the examination, analyzed and interpreted the data. H Yong, CQ Zhang, K Kang, YY Yang, ZC Huang, SE Wang and HT Ge contributed to the acquisition of data. FY Song was responsible for conception and design of the work. All authors read and approved the final manuscript.

Acknowledgments

The authors want to thank Translational Medicine Core Facility of Shandong University for consultation and instrument availability that supported this work, LH Yu and WW Zheng for their assistance in experiments, WH Yu and ZQ Yu for their generous help in data analysis.

References

1. Waller A. Experiments on the Section of the Glosso-Pharyngeal and Hypoglossal Nerves of the Frog, and Observations of the Alterations Produced Thereby in the Structure of Their Primitive Fibres. Edinburgh medical and surgical journal. 1851;76(189):369–76.
2. Perry VH, Brown MC, Lunn ER, Tree P, Gordon S. Evidence that Very Slow Wallerian Degeneration in C57BL/Ola Mice is an Intrinsic Property of the Peripheral Nerve. Eur J Neurosci. 1990;2(9):802–8.
3. Perry VH, Brown MC, Lunn ER. Very Slow Retrograde and Wallerian Degeneration in the CNS of C57BL/Ola Mice. Eur J Neurosci. 1991;3(1):102–5.
4. Lyon MF, Ogunkolade BW, Brown MC, Atherton DJ, Perry VH. A gene affecting Wallerian nerve degeneration maps distally on mouse chromosome 4. Proceedings of the National Academy of Sciences of the United States of America. 1993;90(20):9717–20.
5. Desbois M, Crawley O, Evans PR, Baker ST, Masuho I, Yasuda R, et al. PAM forms an atypical SCF ubiquitin ligase complex that ubiquitinates and degrades NMNAT2. The Journal of biological chemistry. 2018;293(36):13897–909.

6. Babetto E, Beirowski B, Russler EV, Milbrandt J, DiAntonio A. The Phr1 ubiquitin ligase promotes injury-induced axon self-destruction. Cell Rep. 2013;3(5):1422–9.
7. Figley MD, Gu W, Nanson JD, Shi Y, Sasaki Y, Cunnea K, et al. SARM1 is a metabolic sensor activated by an increased NMN/NAD+ ratio to trigger axon degeneration. Neuron. 2021.
8. Essuman K, Summers DW, Sasaki Y, Mao X, DiAntonio A, Milbrandt J. The SARM1 Toll/Interleukin-1 Receptor Domain Possesses Intrinsic NAD(+) Cleavage Activity that Promotes Pathological Axonal Degeneration. Neuron. 2017;93(6):1334-43.e5.
9. Gerdts J, Summers DW, Milbrandt J, DiAntonio A. Axon Self-Destruction: New Links among SARM1, MAPKs, and NAD+ Metabolism. Neuron. 2016;89(3):449–60.
10. Meijer AH, Gabby Krens SF, Medina Rodriguez IA, He S, Bitter W, Ewa Snaar-Jagalska B, et al. Expression analysis of the Toll-like receptor and TIR domain adaptor families of zebrafish. Mol Immunol. 2004;40(11):773–83.
11. Mink M, Fogelgren B, Olszewski K, Maroy P, Csiszar K. A novel human gene (SARM) at chromosome 17q11 encodes a protein with a SAM motif and structural similarity to Armadillo/beta-catenin that is conserved in mouse, Drosophila, and Caenorhabditis elegans. Genomics. 2001;74(2):234–44.
12. Belinda LW, Wei WX, Hanh BT, Lei LX, Bow H, Ling DJ. SARM: a novel Toll-like receptor adaptor, is functionally conserved from arthropod to human. Mol Immunol. 2008;45(6):1732–42.
13. Couillault C, Pujol N, Reboul J, Sabatier L, Guichou JF, Kohara Y, et al. TLR-independent control of innate immunity in Caenorhabditis elegans by the TIR domain adaptor protein TIR-1, an ortholog of human SARM. Nat Immunol. 2004;5(5):488–94.
14. Panneerselvam P, Singh Laishram P, Ho B, Chen J, Ding Jeak L. Targeting of pro-apoptotic TLR adaptor SARM to mitochondria: definition of the critical region and residues in the signal sequence. Biochem J. 2012;442(2):263–71.
15. Santidrian AF, Matsuno-Yagi A, Ritland M, Seo BB, LeBoeuf SE, Gay LJ, et al. Mitochondrial complex I activity and NAD+/NADH balance regulate breast cancer progression. J Clin Invest. 2013;123(3):1068–81.
16. Di Lisa F, Ziegler M. Pathophysiological relevance of mitochondria in NAD(+) metabolism. FEBS Lett. 2001;492(1-2):4–8.
17. Nikiforov A, Dölle C, Niere M, Ziegler M. Pathways and subcellular compartmentation of NAD biosynthesis in human cells: from entry of extracellular precursors to mitochondrial NAD generation. The Journal of biological chemistry. 2011;286(24):21767–78.
18. Loreto A, Di Stefano M, Gering M, Conforti L. Wallerian Degeneration Is Executed by an NMN-SARM1-Dependent Late Ca(2+) Influx but Only Modestly Influenced by Mitochondria. Cell Rep. 2015;13(11):2539–52.
19. Pennisi M, Malaguarnera G, Puglisi V, Vinciguerra L, Vacante M, Malaguarnera M. Neurotoxicity of acrylamide in exposed workers. Int J Environ Res Public Health. 2013;10(9):3843–54.
20. Tareke E, Rydberg P, Karlsson P, Eriksson S, Törnqvist M. Analysis of acrylamide, a carcinogen formed in heated foodstuffs. J Agric Food Chem. 2002;50(17):4998–5006.

21. Schettgen T, Weiss T, Drexler H, Angerer J. A first approach to estimate the internal exposure to acrylamide in smoking and non-smoking adults from Germany. Int J Hyg Environ Health. 2003;206(1):9–14.
22. Urban M, Kavvadias D, Riedel K, Scherer G, Tricker AR. Urinary mercapturic acids and a hemoglobin adduct for the dosimetry of acrylamide exposure in smokers and nonsmokers. Inhal Toxicol. 2006;18(10):831–9.
23. Lantz I, Ternité R, Wilkens J, Hoenicke K, Guenther H, van der Stegen GH. Studies on acrylamide levels in roasting, storage and brewing of coffee. Mol Nutr Food Res. 2006;50(11):1039–46.
24. Spencer PS, Schaumburg HH. A review of acrylamide neurotoxicity. Part II. Experimental animal neurotoxicity and pathologic mechanisms. Can J Neurol Sci. 1974;1(3):152–69.
25. Deng H, He F, Zhang S, Calleman CJ, Costa LG. Quantitative measurements of vibration threshold in healthy adults and acrylamide workers. Int Arch Occup Environ Health. 1993;65(1):53–6.
26. Garland TO, Patterson MW. Six cases of acrylamide poisoning. Br Med J. 1967;4(5572):134–8.
27. He FS, Zhang SL, Wang HL, Li G, Zhang ZM, Li FL, et al. Neurological and electroneuromyographic assessment of the adverse effects of acrylamide on occupationally exposed workers. Scand J Work Environ Health. 1989;15(2):125–9.
28. Edwards PM, Parker VH. A simple, sensitive, and objective method for early assessment of acrylamide neuropathy in rats. Toxicol Appl Pharmacol. 1977;40(3):589–91.
29. Kuperman AS. Effects of acrylamide on the central nervous system of the cat. J Pharmacol Exp Ther. 1958;123(3):180–92.
30. Fullerton PM, Barnes JM. Peripheral neuropathy in rats produced by acrylamide. British journal of industrial medicine. 1966;23(3):210–21.
31. Hopkins A. The effect of acrylamide on the peripheral nervous system of the baboon. J Neurol Neurosurg Psychiatry. 1970;33(6):805–16.
32. Hopkins AP, Gilliatt RW. Motor and sensory nerve conduction velocity in the baboon: normal values and changes during acrylamide neuropathy. J Neurol Neurosurg Psychiatry. 1971;34(4):415–26.
33. Sumner AJ, Asbury AK. Acrylamide neuropathy: selective vulnerability of sensory fibers. Transactions of the American Neurological Association. 1974;99:79–83.
34. Sumner AJ, Asbury AK. Physiological studies of the dying-back phenomenon. Muscle stretch afferents in acrylamide neuropathy. Brain. 1975;98(1):91–100.
35. Erkekoglu P, Baydar T. Acrylamide neurotoxicity. Nutr Neurosci. 2014;17(2):49–57.
36. Clifton GL, Jiang JY, Lyeth BG, Jenkins LW, Hamm RJ, Hayes RL. Marked protection by moderate hypothermia after experimental traumatic brain injury. Journal of cerebral blood flow and metabolism: official journal of the International Society of Cerebral Blood Flow and Metabolism. 1991;11(1):114–21.
37. Monville C, Torres EM, Dunnett SB. Comparison of incremental and accelerating protocols of the rotarod test for the assessment of motor deficits in the 6-OHDA model. J Neurosci Methods.

2006;158(2):219–23.

38. Youssef AF, Santi BW. Simple Neurobehavioral Functional Observational Battery and Objective Gait Analysis Validation by the Use of Acrylamide and Methanol with a Built-In Recovery Period. Environ Res. 1997;73(1):52–62.
39. Moser VC, Anthony DC, Sette WF, MacPhail RC. Comparison of subchronic neurotoxicity of 2-hydroxyethyl acrylate and acrylamide in rats. Fundam Appl Toxicol. 1992;18(3):343–52.
40. LoPachin RM, Ross JF, Reid ML, Das S, Mansukhani S, Lehning EJ. Neurological Evaluation of Toxic Axonopathies in Rats: Acrylamide and 2,5-Hexanedione. Neurotoxicology. 2002;23(1):95–110.
41. Takeuchi Y, Ono Y, Hisanaga N, Kitoh J, Sugiura Y. A comparative study on the neurotoxicity of n-pentane, n-hexane, and n-heptane in the rat. British journal of industrial medicine. 1980;37(3):241–7.
42. Lima RT, Sousa D, Paiva AM, Palmeira A, Barbosa J, Pedro M, et al. Modulation of Autophagy by a Thioxanthone Decreases the Viability of Melanoma Cells. Molecules (Basel, Switzerland). 2016;21(10).
43. Kong FJ, Wu JH, Sun SY, Zhou JQ. The endoplasmic reticulum stress/autophagy pathway is involved in cholesterol-induced pancreatic β-cell injury. Scientific reports. 2017;7:44746.
44. Schindelin J, Arganda-Carreras I, Frise E, Kaynig V, Longair M, Pietzsch T, et al. Fiji: an open-source platform for biological-image analysis. Nat Methods. 2012;9(7):676–82.
45. Hayakawa T, Kato K, Hayakawa R, Hisamoto N, Matsumoto K, Takeda K, et al. Regulation of anoxic death in Caenorhabditis elegans by mammalian apoptosis signal-regulating kinase (ASK) family proteins. Genetics. 2011;187(3):785–92.
46. Kim Y, Zhou P, Qian L, Chuang J-Z, Lee J, Li C, et al. MyD88-5 links mitochondria, microtubules, and JNK3 in neurons and regulates neuronal survival. The Journal of experimental medicine. 2007;204(9):2063–74.
47. Mukherjee P, Winkler CW, Taylor KG, Woods TA, Nair V, Khan BA, et al. SARM1, Not MyD88, Mediates TLR7/TLR9-Induced Apoptosis in Neurons. Journal of immunology (Baltimore, Md: 1950). 2015;195(10):4913-21.
48. Killackey SA, Rahman MA, Soares F, Zhang AB, Abdel-Nour M, Philpott DJ, et al. The mitochondrial Nod-like receptor NLRX1 modifies apoptosis through SARM1. Mol Cell Biochem. 2019;453(1):187–96.
49. Gerdts J, Summers DW, Sasaki Y, DiAntonio A, Milbrandt J. Sarm1-mediated axon degeneration requires both SAM and TIR interactions. J Neurosci. 2013;33(33):13569–80.
50. Geisler S, Doan RA, Cheng GC, Cetinkaya-Fisgin A, Huang SX, Höke A, et al. Vincristine and bortezomib use distinct upstream mechanisms to activate a common SARM1-dependent axon degeneration program. JCI Insight. 2019;4(17):e129920.
51. Bosanac T, Hughes RO, Engber T, Devraj R, Brearley A, Danker K, et al. Pharmacological SARM1 inhibition protects axon structure and function in paclitaxel-induced peripheral neuropathy. Brain. 2021.

52. Prats E, Gómez-Canela C, Ben-Lulu S, Ziv T, Padrós F, Tornero D, et al. Modelling acrylamide acute neurotoxicity in zebrafish larvae. Scientific reports. 2017;7(1):13952.
53. MacAskill AF, Kittler JT. Control of mitochondrial transport and localization in neurons. Trends Cell Biol. 2010;20(2):102–12.
54. Chen H, Chan DC. Mitochondrial dynamics–fusion, fission, movement, and mitophagy–in neurodegenerative diseases. Hum Mol Genet. 2009;18(R2):R169-76.
55. Schon EA, Przedborski S. Mitochondria: the next (neurode)generation. Neuron. 2011;70(6):1033–53.
56. Chan DC. Mitochondria: dynamic organelles in disease, aging, and development. Cell. 2006;125(7):1241–52.
57. Ravikumar B, Vacher C, Berger Z, Davies JE, Luo S, Oroz LG, et al. Inhibition of mTOR induces autophagy and reduces toxicity of polyglutamine expansions in fly and mouse models of Huntington disease. Nat Genet. 2004;36(6):585–95.
58. Pickford F, Masliah E, Britschgi M, Lucin K, Narasimhan R, Jaeger PA, et al. The autophagy-related protein beclin 1 shows reduced expression in early Alzheimer disease and regulates amyloid beta accumulation in mice. J Clin Invest. 2008;118(6):2190–9.
59. Yang Y, Chen S, Zhang J, Li C, Sun Y, Zhang L, et al. Stimulation of autophagy prevents amyloid-β peptide-induced neuritic degeneration in PC12 cells. Journal of Alzheimer's disease: JAD. 2014;40(4):929–39.
60. Clarke JP, Mearow K. Autophagy inhibition in endogenous and nutrient-deprived conditions reduces dorsal root ganglia neuron survival and neurite growth in vitro. J Neurosci Res. 2016;94(7):653–70.
61. Wang Y, Song M, Song F. Neuronal autophagy and axon degeneration. Cell Mol Life Sci. 2018;75(13):2389–406.
62. Kim I, Rodriguez-Enriquez S, Lemasters JJ. Selective degradation of mitochondria by mitophagy. Archives of biochemistry and biophysics. 2007;462(2):245–53.
63. Han S, Jeong YY, Sheshadri P, Su X, Cai Q. Mitophagy regulates integrity of mitochondria at synapses and is critical for synaptic maintenance. EMBO reports. 2020;21(9):e49801.
64. Kim I, Lemasters JJ. Mitophagy selectively degrades individual damaged mitochondria after photoirradiation. Antioxid Redox Signal. 2011;14(10):1919–28.
65. Pollock L, Jardine J, Urbé S, Clague MJ. The PINK1 repertoire: Not just a one trick pony. Bioessays. 2021;43(11):e2100168.
66. Murata H, Sakaguchi M, Kataoka K, Huh N-H. SARM1 and TRAF6 bind to and stabilize PINK1 on depolarized mitochondria. Molecular biology of the cell. 2013;24(18):2772–84.

Figures

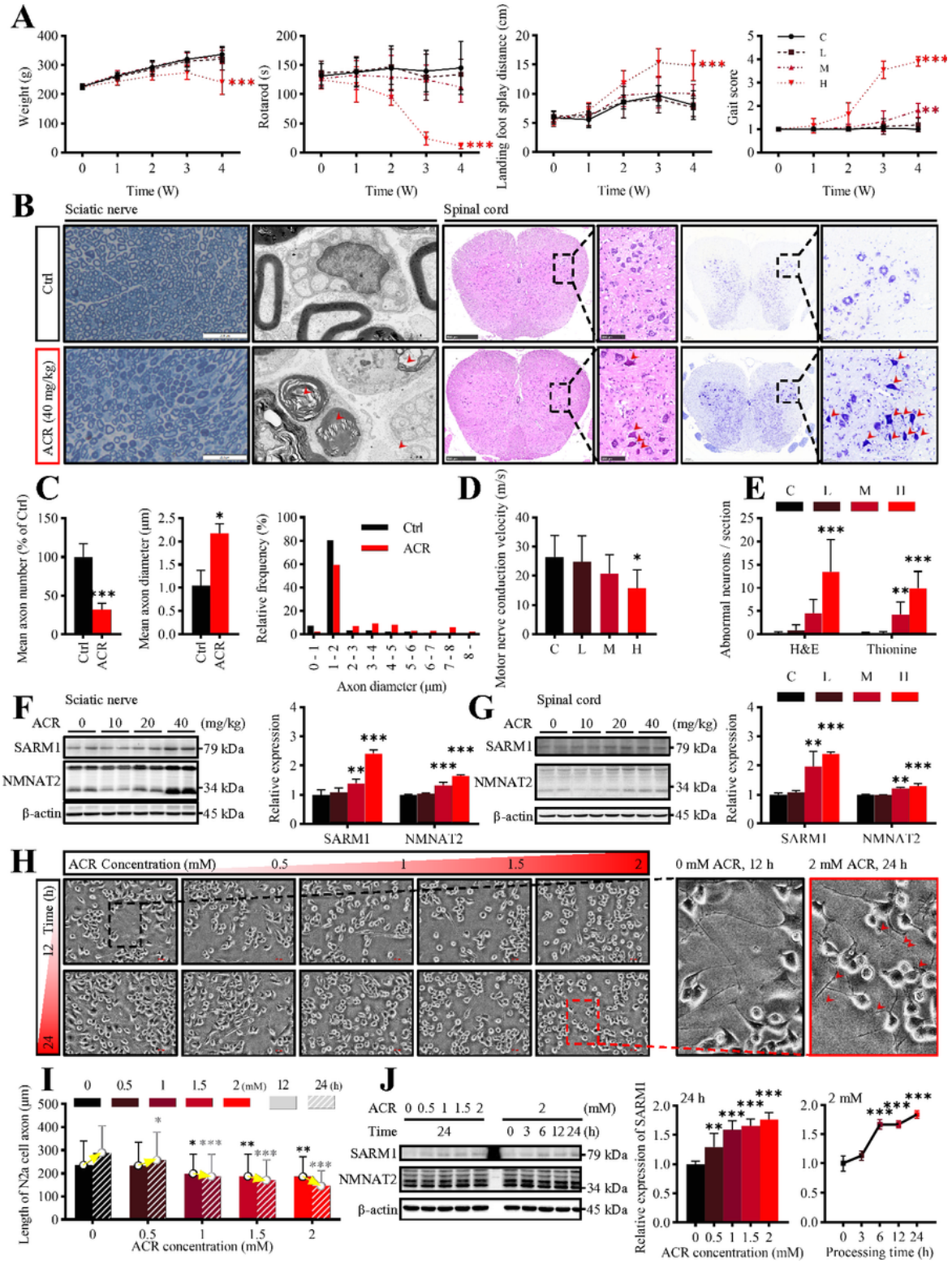

Figure 1

ACR induces Wallerian-like degeneration and upregulates SARM1. (A) Body weight and neurobehavioral performances of rats subjected to ACR for four weeks. (B) Axon damage and neuronal morphology changes in rats. Red arrowheads in the transmission electron microscope images of the sciatic nerve indicate demyelinated axons. Red arrowheads in the spinal cord H&E and Thionine Nissl staining images indicate abnormal α motor neurons. (C) Quantification of axon number, axon diameter, and distribution of

axon diameter in the sciatic nerve. (D) Neurophysiological tests of rats subjected to ACR for four weeks. (E) Quantification of α motor neurons with abnormal morphological changes. (F) Western blotting analysis of Wallerian degeneration-related proteins in the sciatic nerve and (G) in the spinal cord from rats subjected to ACR for four weeks. (H) Representative images and axon length measurement results (I) of N2a cells processed by ACR for different concentrations and different time. Red arrowheads indicate the damaged axons that are accompanied by swelling, blebbing, and fragmentation. Scale bar, 100 μm. (J) Western blotting analysis of Wallerian degeneration-related proteins in N2a cells with ACR treated for different concentrations and different time.

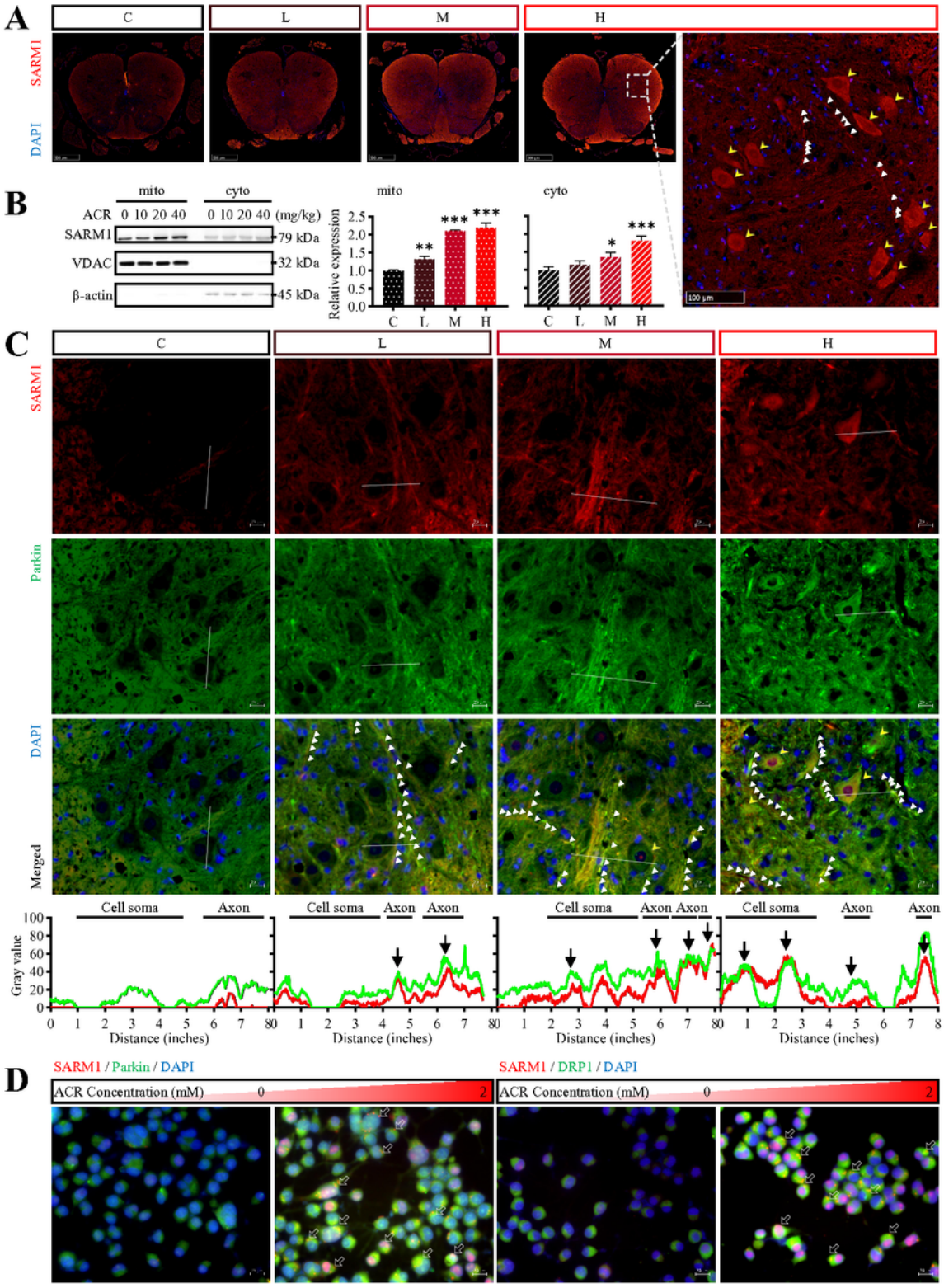

Figure 2

SARM1, which is up-regulated in ACR neuropathy, accumulates on mitochondria. (A) Representative immunofluorescence images of SARM1 in the spinal cord sections from rats subjected to ACR for four weeks. In the detail display, yellow and white arrowheads refer to the gathered SARM1 in the cell soma and axon, respectively. (B) Western blotting analysis of SARM1. The mitochondrial fraction and the cytoplasmic fraction of the same sample are loaded (40 μg per channel) in the same gel for

immunoblotting. And sequentially incubate with primary anti-SARM1, anti-VDAC, anti-β-actin antibodies. VDAC and β-actin are used for internal control and homogenization of mitochondrial fractions and cytoplasmic fractions, respectively. (C) Immunofluorescence of SARM1 (red) and Parkin (green) in spinal cord sections from rats subjected to ACR for four weeks. The white lines in the images are the region of interest for gray intensity analysis of red and green channels. Black arrows indicate overlapped points. Scale bar, 20 μm. (D) Immunofluorescence of SARM1 (red) and Parkin (green), SARM1 (red) and DRP1 (green) in N2a cells with ACR treated for 24 h. The hollow white arrows indicate the punctate-accumulated SARM1. Scale bar, 20 μm.

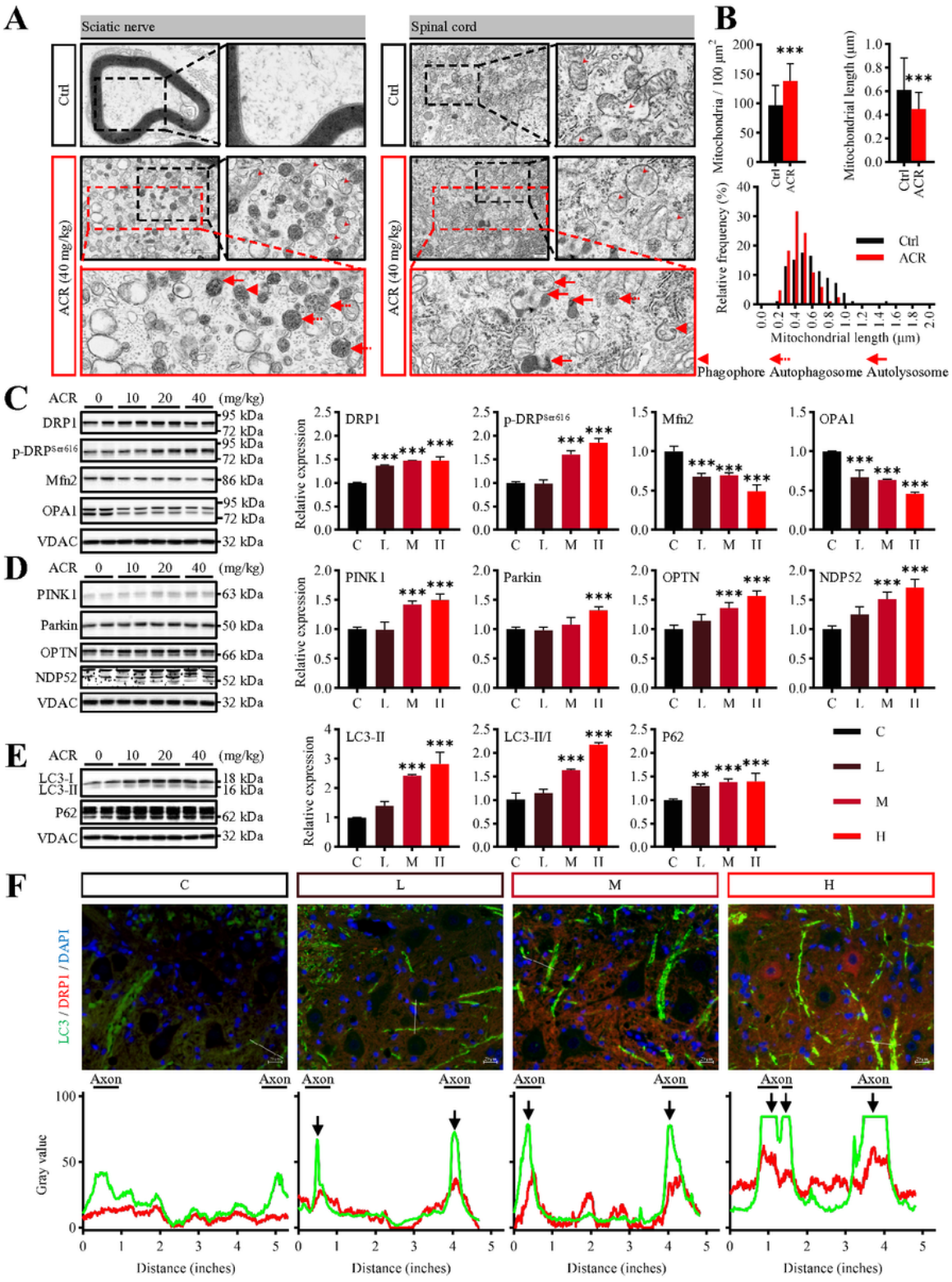

Figure 3

Mitochondrial dynamics are disturbed and mitophagy-related proteins are upregulated in ACR neuropathy. (A) Representative transmission electron microscopy images of the sciatic nerve and the spinal cord from rats subjected to ACR for four weeks. The black and red dotted boxes show the ultrastructure of mitochondria and autophagy-related vesicles, respectively. (B) Quantification of mitochondrial number, mitochondrial length, and distribution of mitochondrial length in the spinal cord of

rats subjected to ACR for four weeks. (C) Western blotting analysis of mitochondrial dynamic- (D) mitophagy- and (E) autophagy-related proteins in the spinal cord from rats subjected to ACR for four weeks. (F) Immunofluorescence of LC3 (green) and DRP1 (red) in the spinal cord sections from rats subjected to ACR for four weeks. The white lines in the images are the region of interest for gray intensity analysis of red and green channels. Black arrows indicate overlapped points. Scale bar, 20 μm.

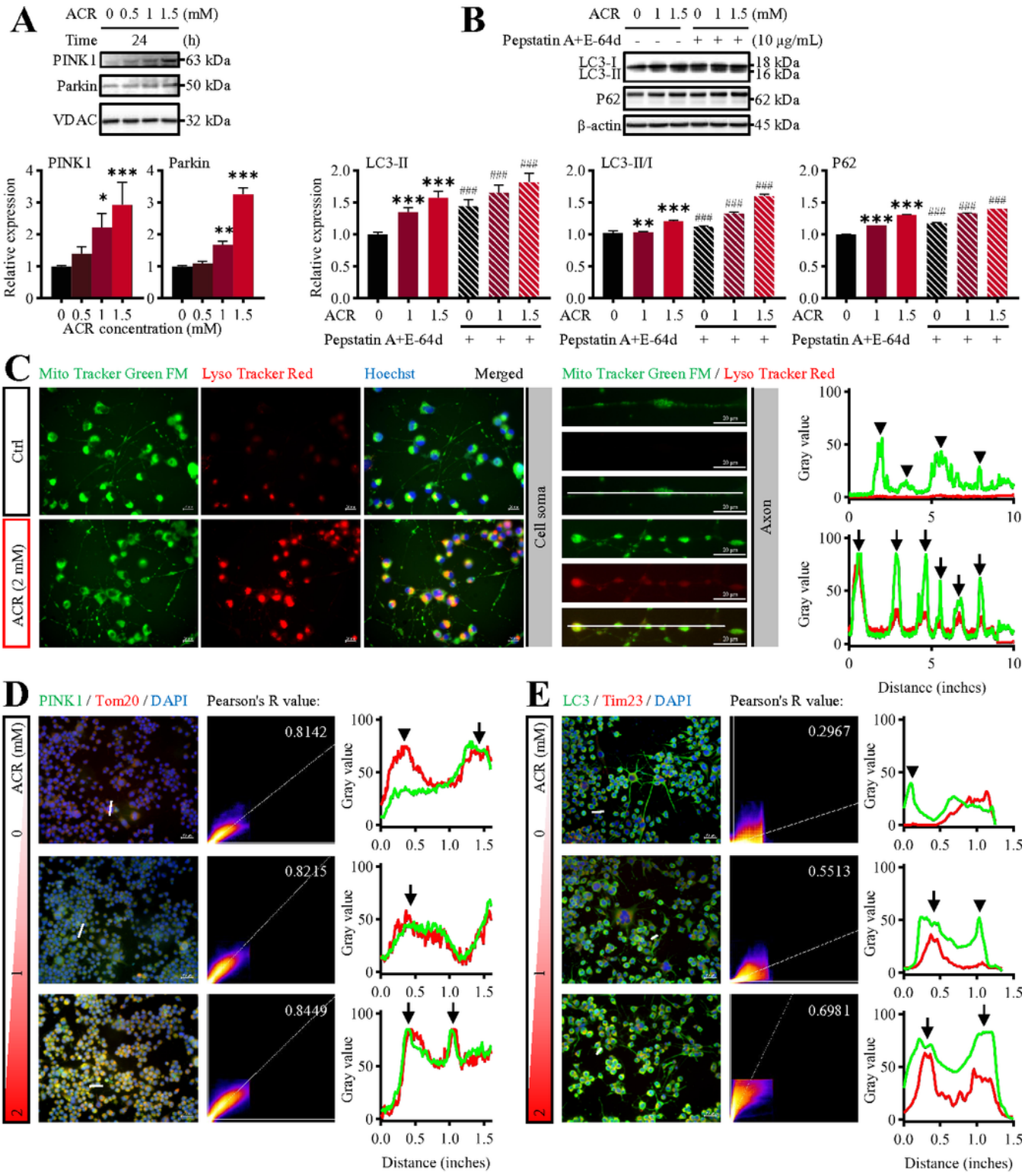

Figure 4

Mitophagy is activated in ACR neuropathy. (A) Western blotting analysis of mitophagy-related proteins in ACR processed N2a cells. (B) Western blotting analysis of LC3 turnover experiment. (C) Live cell imaging of N2a cells with ACR treated for 24 h or not. Scale bar, 20 μm. (D) Immunofluorescence of PINK1 (green) and Tom20 (red), (E) LC3 (green) and Tim23 (red) in N2a cells with ACR treated for 24 h. Scale bar, 50 μm. The white lines in the images are the region of interest for gray intensity analysis of red and green channels. Black arrows indicate overlapped points, and black arrowheads indicate non-co-located points.

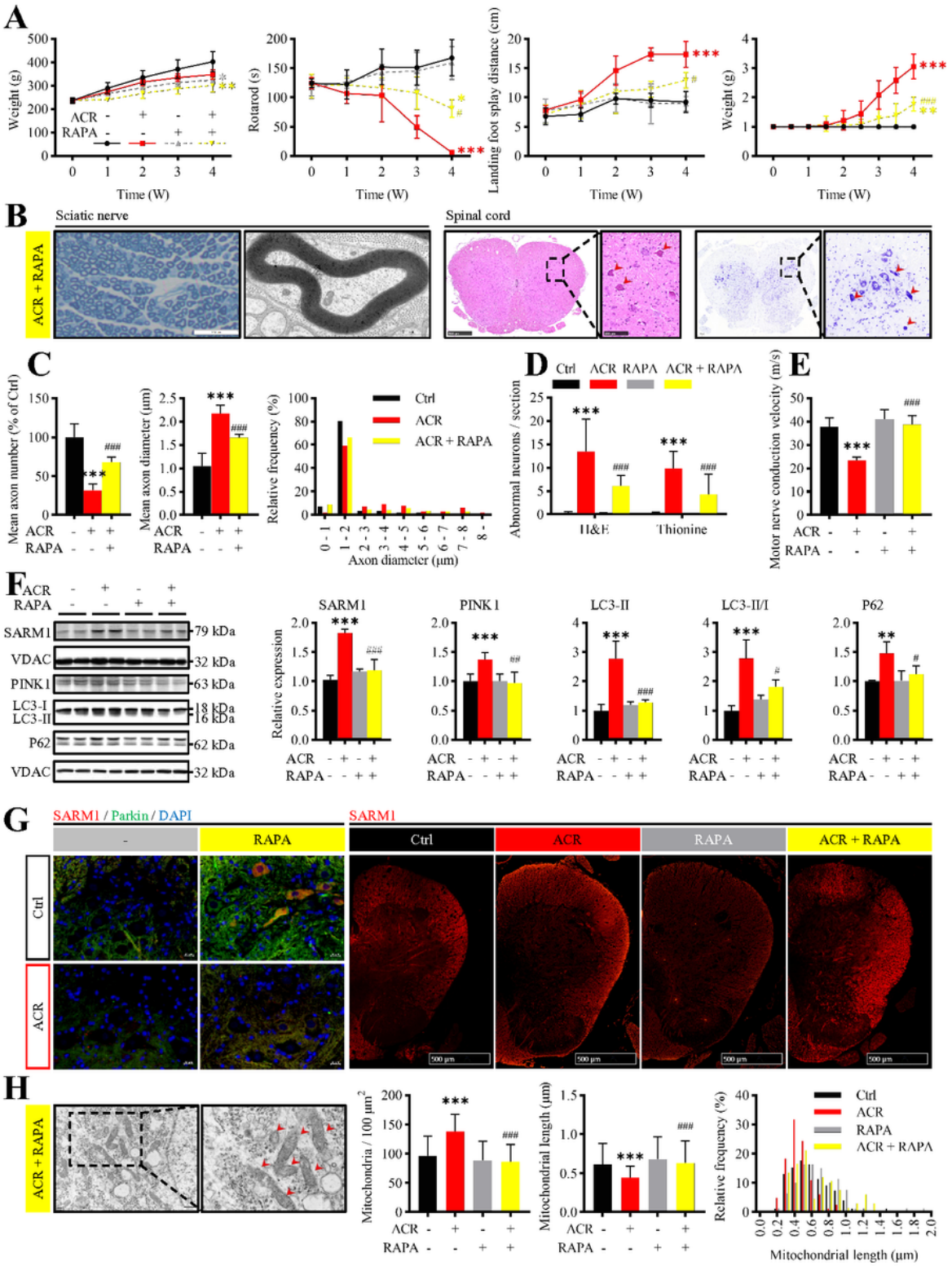

Figure 5

Rapamycin limits the mitochondrial accumulation of SARM1 and rescues the phenotype of ACR poisoning. (A) Body weight and neurobehavioral performances of rats. (B) Axon damage and neuronal morphology changes in rats with RAPA intervened. Red arrowheads in the spinal cord H&E and Thionine Nissl staining images indicate abnormal α motor neurons. (C) Quantification of axon number, axon diameter, and distribution of axon diameter in the spinal cord of rats with RAPA intervened for four weeks. (D) Quantification of α motor neurons with abnormal morphological changes. (E) Neurophysiological tests of rats with RAPA intervened or not. (F) Western blotting analysis of SARM1 and mitophagy-related proteins in the spinal cord. (G) Immunofluorescence of SARM1 (red) and Parkin (green) and representative immunofluorescence images of SARM1 in the spinal cord sections. (H) Representative transmission electron microscopy images of the spinal cord from rats with RAPA intervened or not. The black dotted box shows the mitochondria ultrastructure. Histograms on the right are quantification of mitochondrial number, mitochondrial length, and distribution of mitochondrial length in the spinal cord of rats with RAPA intervened or not.

Supplementary Files

This is a list of supplementary files associated with this preprint. Click to download.

- GraphicalAbstract.pdf
- Additionalfile1.Reagent.xlsx
- Additionalfile2.Originalblots.pptx
- Additionalfile3.Statisticalanalyses.xlsx
- Additionalfile4.Supplementaryfigures.pdf